

A robust motion estimation algorithm for PIV

Mani Thomas¹, Shubhra Misra², Chandra Kambhamettu¹
and James T Kirby²

¹ Video/Image Modeling and Synthesis Lab, Department of Computer and Information Sciences, University of Delaware, Newark, DE, USA

² Center for Applied Coastal Research, Department of Civil and Environmental Engineering, University of Delaware, Newark, DE, USA

E-mail: mani@udel.edu

Received 6 September 2004, in final form 1 December 2004

Published 17 February 2005

Online at stacks.iop.org/MST/16/865

Abstract

The present study proposes an approach for robust estimation of the instantaneous motion field from a time-lagged pair of PIV images. The method is based on phase correlation, where the phase of the Fourier components is used for motion parameter estimation. Unlike the cross correlation-based techniques, this technique uses ‘whitening’ FIR filters to sharpen the cross correlation maxima, thereby improving the accuracy of identification of the peak. The proposed method also combines the advantages of the phase correlation and the cross correlation techniques in determining the reliability of the estimates, thus providing a method of filtering out a significantly large number of spurious vectors. This reliability metric helps reduce the possibility of over-smoothing the flow field when performing data validation. With regard to the efficiency of the technique, both phase correlation and cross correlation are derived from the Fourier components of the same image region. Each of the estimates can thus be obtained in parallel, without increasing the computational complexity of the system. Unlike many region-based methods that are currently available, the entire motion is decomposed as a global and a local motion field, which helps accurately obtain high interrogation resolution estimates for the local motion field.

Keywords: PIV, motion estimation, phase correlation, cross correlation, image multi-scale hierarchy

(Some figures in this article are in colour only in the electronic version)

1. Introduction

Particle image velocimetry (PIV) is a non-intrusive measurement technique used to obtain spatially dense maps of instantaneous velocities from time-lagged images of a flow field [1]. As described by Christensen [9], the main advantage of using PIV in studying complex flow phenomena is that PIV can be used to measure two- or three-dimensional instantaneous flow over a planar domain.

In a regular PIV experiment, the flow is seeded with tracer particles and illuminated with a sheet or volume of light from a pulsed laser. The light scattered off from the particles is

captured in the form of a moving pattern, an analysis of which provides an accurate measure of the flow [32].

Typically, algorithms that have been developed for the analysis of moving patterns of tracer particles are region-based methods that compute the cross correlation between the interrogation regions obtained from the two images [2, 43]. Region-based techniques estimate the average motion of small groups of particles, thereby making the method noise tolerant and robust [28]. Among the various modifications to the region-based method, Scarano and Riethmuller [35] proposed an algorithm where the displacement is predicted and corrected by means of an iterative procedure. As reported by the authors,

the window displacement iterative multigrid (WiDIM) method is extremely robust due to the use of this iterative prediction-correction scheme. The method proposed in this paper is very similar to the WiDIM method; however it has an additional advantage wherein the total motion is decomposed into a global motion field and a local motion field. This increases the robustness in the estimation of the moving patterns of the tracer particles.

Unlike the region-based methods, where the intra-region motion is assumed to be accurately modelled as a translation of coherent groups of particles, the intensity-based differential methods [31] estimate the motion via the optic flow equation (equation (1)). The motion parameters are extracted using some form of regularization such as smoothness of the flow field. In [12], Corpetti *et al* discuss a minimization-based motion estimation algorithm for fluids based on the brightness constancy equation and fluid dynamics based regularization parameters. The biggest disadvantage with the differential methods is the requirement of strong gradient information in the images for the displacement estimates to be accurate. In synthetic images, this condition can be easily fulfilled but in real images this requirement is frequently violated leading to inaccurate results.

The estimation of motion in most PIV experiments has been found to suffer from many bias errors [9]. ‘Peak Locking’ errors are the most significant, where particle displacements are biased towards full or half pixel values and it arises mainly due to the choice of the sub-pixel estimator. As peak-locking presents a serious limitation to the performance of any digital PIV system, a number of solutions have been put forth. Gui and Wereley [15] introduced a window-shift technique to reduce the peak locking effect. The proposed method estimates very small particle image displacements by continuously shifting the interrogation window and using bilinear interpolation of the grey values, along with a correlation-based interrogation method. In spite of the improved accuracy attained by this method, the biggest disadvantage is the increase in computational complexity in interpolating the grey scale values.

In handling the peak locking problem, Westerweel [42] showed that the Gaussian sub-pixel estimator was better than the quadratic. Marxen *et al* [25] compared the Gaussian particle centre estimator for the particle tracking velocimetry using the analytical solution and the least-squares Gaussian parameter estimation. It was found that the analytical solution for sub-pixel estimation using a 3-point Gaussian behaved like the least-squares parameter estimation framework with a minimum position error of 0.03 pixels. The authors recommended the use of the analytical solution since the computation was 100 times faster than the least-squares fit. Roesgen [34] recently presented the ‘sinc’ kernel for estimating the sub-pixel displacements, and showed that the bias errors were completely suppressed. Despite the apparent efficiency of the kernel in suppressing the bias errors, there is a sparsity of research in utilizing the ‘sinc’ kernel to remove bias errors and further investigation would be beneficial. In developing our algorithm, we have used the analytical Gaussian sub-pixel estimator and the comparative results with the ground truth vectors indicate minimal bias errors.

Even with accurate sub-pixel estimators to deal with bias errors, a consequent and almost always necessary post-processing step involves the detection and replacement of spurious displacements that arise from image ‘noise’ or deficiencies in the evaluation method [41, 32]. For example, the occurrence of spurious vectors can result from a locally low particle image density or background noise from reflections [18]. In [26], Nogueira *et al* describe various post-processing steps for validating the estimated displacements in a PIV experiment and also provide algorithms for the correction of spurious vectors using interpolating filters. In the PIV validation technique presented by Green *et al* [14], forward and reverse projected vectors are computed at chosen analysis points and the projected vectors are used to test the validity of the vector estimated at the analysis point. This coherence-based validation scheme provides accurate results. However, the estimation of the forward and reverse projected vectors causes a three-fold increase in the computational complexity.

In this paper, we present a method that estimates the motion by first computing a global motion field and then uses the global motion field as an initialization in estimating the local motion. This decomposition into a two-level hierarchy of flow estimation helps achieve very high spatial resolution accurately. The global motion field is estimated using phase correlation [38] while the local motion is obtained using a robust voting scheme composed of phase correlation and cross correlation in order to accurately identify possible spurious vectors.

The organization of the paper is as follows. In section 2, we describe the motion estimation technique that is being used. This is followed by the details of the implementation where the global and local motion estimation modules are described. The results of the experiments with the standardized images from JPIV [27] and the PIV Challenge 2001 [37] are presented to test the validity of the scheme.

2. Motion estimation techniques

When a time-lagged pair of images is viewed under the constraint of a small spatio-temporal difference, the ‘correspondence problem’ can be cast as the problem of estimating the apparent motion of the image brightness pattern [39]. Estimating this apparent motion or the optic flow leads to the fundamental equation of motion analysis, the image brightness constancy assumption, $\frac{dE(x,y,t)}{dt} = 0$, where $E(x, y, t)$ is the image intensity, (x, y) are the spatial coordinates and t is the time.

The first-order Taylor expansion of the brightness constancy assumption gives the optic flow equation,

$$\frac{\partial E}{\partial x} \frac{dx}{dt} + \frac{\partial E}{\partial y} \frac{dy}{dt} + \frac{\partial E}{\partial t} \approx 0 \quad (1)$$

where $\frac{dx}{dt}$ and $\frac{dy}{dt}$ are the components of the motion to be estimated from the image pair. Under the assumption of small temporal resolution, the optic flow equation is considered valid and many techniques have been developed to estimate the apparent flow field between the two images [17].

Among the various techniques developed, differential techniques derive directly from (1). Due to inherent difficulties in performing numerical differentiation, region-based matching techniques provide a possible alternative in

estimating the displacement vector field [5]. This is done by either minimizing an error criterion such as ‘sum of squared difference’ (ε), or maximizing a similarity measure such as ‘normalized cross correlation’ (ρ) between the current image block and potential candidates within a predefined search window in the previous frame.

$$\varepsilon = \sum_{\mathbf{x}, \mathbf{x}'} [E(\mathbf{x}, t) - E(\mathbf{x}', t + \Delta t)]^2 \quad (2)$$

$$\rho = \frac{\sum [E(\mathbf{x}, t) - \overline{E(\mathbf{x}, t)}][E(\mathbf{x}', t + \Delta t) - \overline{E(\mathbf{x}', t + \Delta t)}]}{\sqrt{\sum [E(\mathbf{x}, t) - \overline{E(\mathbf{x}, t)}]^2 \sum [E(\mathbf{x}', t + \Delta t) - \overline{E(\mathbf{x}', t + \Delta t)}]^2}} \quad (3)$$

where \mathbf{x} and \mathbf{x}' are the spatial positions in the time-lagged (Δt) images, $\overline{E(\cdot)}$ is the mean of the region under consideration and \sum is defined over all $\mathbf{x}' (\mathbf{x}' = \mathbf{x} + \mathbf{d})$ within a predefined search window with \mathbf{d} being the displacement to be estimated. The phase correlation algorithm presented in section 2.1 falls under the general class of region-based motion estimation.

2.1. Phase correlation

Phase correlation, like cross correlation, is derived from the Fourier shift theorem which states that the time lag of a one-dimensional signal is equivalent to a phase change in the frequency domain. Thus, for two continuous functions $f(\mathbf{x})$ and $g(\mathbf{x})$ in the two-dimensional Euclidean space, related by $g(\mathbf{x}) = f(\mathbf{x} + \mathbf{d})$ where \mathbf{d} is the displacement, the cross correlation between the two can be obtained as the inverse Fourier transform of the product of the individual Fourier transforms

$$\begin{aligned} \mathcal{R}_{fg}(\mathbf{d}) &= \mathcal{F}^{-1}(\mathcal{F}(f(\mathbf{x})) \times \mathcal{F}(g(\mathbf{x}))^*) \\ &= \mathcal{F}^{-1}(F(\mathbf{u})F^*(\mathbf{u})e^{-j2\pi\mathbf{u}^T\mathbf{d}}) \end{aligned} \quad (4)$$

where $F(\mathbf{u})$ and $G(\mathbf{u})$ are the corresponding Fourier transforms of f and g with \star being the complex conjugate and \mathbf{u} being the frequency components in the Fourier space. From the shift theorem, we have $G(\mathbf{u}) = e^{j2\pi\mathbf{u}^T\mathbf{d}}F(\mathbf{u})$.

Given the correlation surface, motion is estimated by finding the position of the maximum. But due to the aperture problem [17], there are situations where the correlation surface contains multiple peaks. Selecting the maximum from the correlation surface in those cases does not provide the best estimate. A solution to this problem is to sharpen the true cross correlation peak by using ‘whitening’ zero-phase FIR filters, $H_1 = |F(\mathbf{u})|$ and $H_2 = |G^*(\mathbf{u})|$ [24]. Thus prior to computing the inverse transform in (4), we eliminate the magnitude components from $F(\mathbf{u})$ and $G^*(\mathbf{u})$ using the FIR filters. This modified correlation equation provides a Dirac delta function centred at the translation parameters, which can be estimated easily and more accurately.

$$\begin{aligned} \wp_{fg}(\mathbf{d}) &= \mathcal{F}^{-1}\left(\frac{F(\mathbf{u})}{H_1} \frac{G^*(\mathbf{u})}{H_2}\right) \\ &= \mathcal{F}^{-1}\left(\frac{F(\mathbf{u})}{|F(\mathbf{u})|} \frac{F^*(\mathbf{u})e^{-j2\pi\mathbf{u}^T\mathbf{d}}}{|F^*(\mathbf{u})|}\right) \\ &= \mathcal{F}^{-1}(e^{-j2\pi\mathbf{u}^T\mathbf{d}}) \\ &= \delta(\mathbf{x} - \mathbf{d}). \end{aligned} \quad (5)$$

Extensive studies on the use of phase correlation for motion estimation have been provided in [38, 40], and in general the technique is extremely robust when estimating large displacements. An important advantage of motion estimation methods based on phase correlation is their insensitivity to illumination variation since the magnitude terms are removed by the whitening filters [24]. Algorithms based on the ‘cross correlation’ metric, however, perform a selection which is biased towards points having higher intensities and thus could provide incorrect displacements represented by local maxima. The phase-based techniques are also characterized by their insensitivity to correlated and frequency-dependent noise which render them robust in the estimation space [13].

The other notable advantage of phase correlation is that the affine parameters, such as rotation, shear and scale, which are coupled in the spatial domain, are separated from the translation components into the magnitude and the phase spectrum respectively in the Fourier domain. This is evident from the affine Fourier theorem as proposed by Bracewell [8], which provides the generalization to the Fourier shift theorem under an affine transformation. Thus, given an affine transformation between the two continuous functions, $g(\mathbf{x}) = f(\mathbf{A}\mathbf{x} + \mathbf{d})$ with \mathbf{d} being the displacement and $\mathbf{A} = \begin{pmatrix} a & b \\ d & e \end{pmatrix}$ being the affine matrix, the relationship governing the Fourier transformation of the two continuous functions is

$$\begin{aligned} G(\mathbf{u}) &= \frac{1}{\Delta} e^{j\frac{2\pi}{\Delta}(\mathbf{u}_A^T\mathbf{d})} \int_{-\infty}^{\infty} \int_{-\infty}^{\infty} f(\mathbf{x}') e^{j\frac{2\pi}{\Delta}(\mathbf{u}_A^T\mathbf{x}')} d\mathbf{x}' \\ &= \frac{1}{\Delta} e^{j\frac{2\pi}{\Delta}(\mathbf{u}_A^T\mathbf{d})} F(\mathbf{u}_A) \end{aligned} \quad (6)$$

where $\Delta = ae - bd = \det(\mathbf{A})$ and $\mathbf{u}_A = \Delta(\mathbf{A}^{-1}\mathbf{u})$. The affine Fourier theorem describes the separation of the affine terms and the linear terms in the frequency space. The estimation of the displacement parameters can thus be performed in the phase spectrum while the parameters of the motion governed by the affine parameters can be estimated from the magnitude spectrum [23, 33, 20].

Under the assumption that the local motion is linear, the affine Fourier theorem gives way to the Fourier shift theorem from which most region-based matching techniques are derived. Thus, in the case where the local motion can be approximated as linear, both cross correlation and phase correlation would have a peak at the correct location. If the underlying motion contains strong affine components, most region-based techniques would provide the average motion of the region that is analysed by the interrogation block. Being a sharpened version of the cross correlation peak, phase correlation is more sensitive to the presence of affine components in the motion field. It thus provides a stronger metric in determining the presence of nonlinear motion within the interrogation block.

This idea forms the basis of our reliability measure, i.e. given the phase correlation peak and the cross correlation peak, the estimate is considered extremely reliable under the cases where the peaks of the two estimated metrics coincide. If the peaks of the two surfaces do not coincide, the region under consideration does not have a unique linear velocity and any linear model would only provide an approximation of the motion.

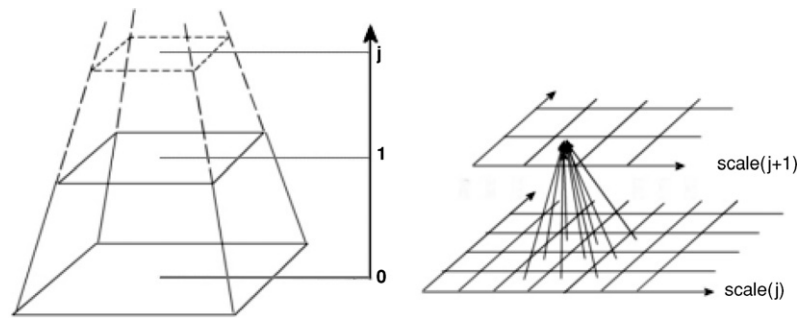


Figure 1. Creation of an image pyramid using a 3×3 filter.

The important advantage of this robust voting scheme is that both the similarity metrics are derived from the Fourier components of the same regions under consideration. Thus performing the 2D fast Fourier transform (FFT) [11] once does not significantly add to the computational complexity over other cross correlation-based techniques.

3. Algorithm and implementation

In computing the optic flow, all techniques face two interdependent problems which arise due to the choice of the analysis window. The smaller the analysis window, the greater are the number of potential candidates that have a high correlation with the interrogation block. On the other hand, there is a higher probability of having a combination of various motions when the window size is large. This problem is called the ‘generalized aperture problem’ and defines the upper bound on the availability of accurate motion estimates at high spatial resolutions [17].

One approach used in dealing with this problem is by handling the motion estimation at multiple resolutions [4, 6]. This enables percolation of information from a coarser resolution to a finer resolution in a computationally efficient fashion. The disadvantage with this hierarchical process is that any motion smaller than the degree of decimation is lost during the process of creation of the resolution hierarchy.

The method implemented here has three processing components. The first component estimates the global motion that is taking place between the image pairs using a multi-resolution image hierarchy [7]. The second component estimates the sub-pixel level local rectilinear motion and the third component performs the outlier removal and data validation.

3.1. Global motion estimation

The global motion field is estimated by performing phase correlation at each level of the image pyramid hierarchy (figure 2). The image pyramid is computed for each image of the image pair using a Gaussian filter followed by a 1:2 signal down sampling. This helps reduce the aliasing artefacts that otherwise arise due to the down sampling [30]. This is shown in figure 1 where a 3×3 neighbourhood is used in creating the image pyramid.

At each level of the pyramid, the down-sampled image pair is divided into a tessellation of blocks and the motion field is computed, by performing phase correlation, over the

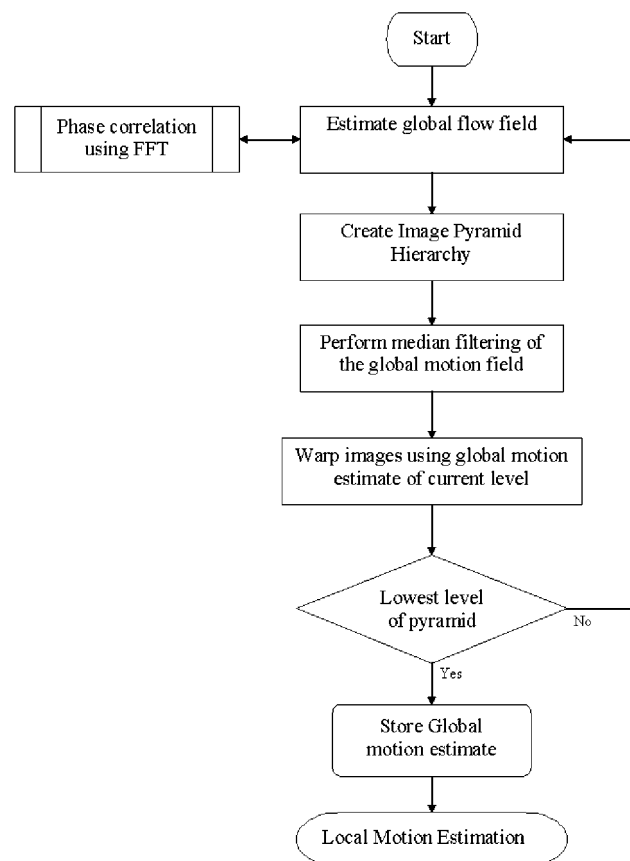


Figure 2. Flow chart for the estimation of the global motion field.

entire tessellation of blocks. The global displacement field so obtained is median filtered to remove spurious vectors before percolating the estimate from the coarser levels of the pyramid towards the finer resolutions. At the finest resolution of the image hierarchy, the global motion field is obtained [3].

Due to the periodic nature of the discrete Fourier transform, the maximum measurable displacement using the Fourier transform of a signal within a window of size W is $W/2$. Thus, to capture translations of magnitude \mathbf{d} , the window size should be at least $2 \max(d_x, d_y)$ where d_x and d_y are the components of the displacement along the two coordinate directions.

3.2. Local motion estimation

The global motion field obtained from the previous stage provides the initial estimate for the local motion estimation.

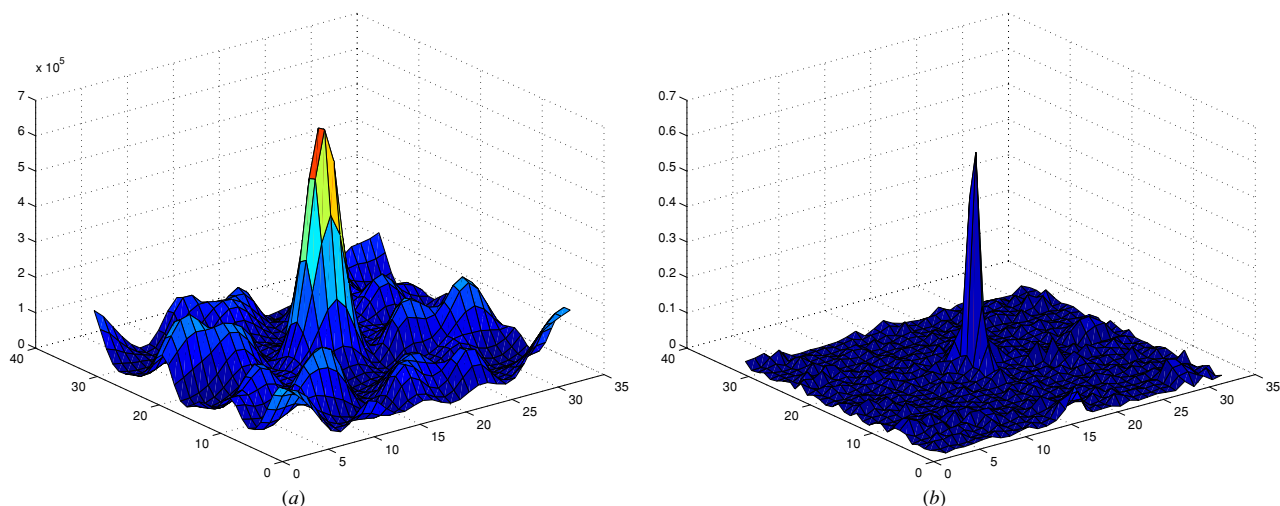


Figure 3. Reliability verification using (a) cross correlation (b) phase correlation.

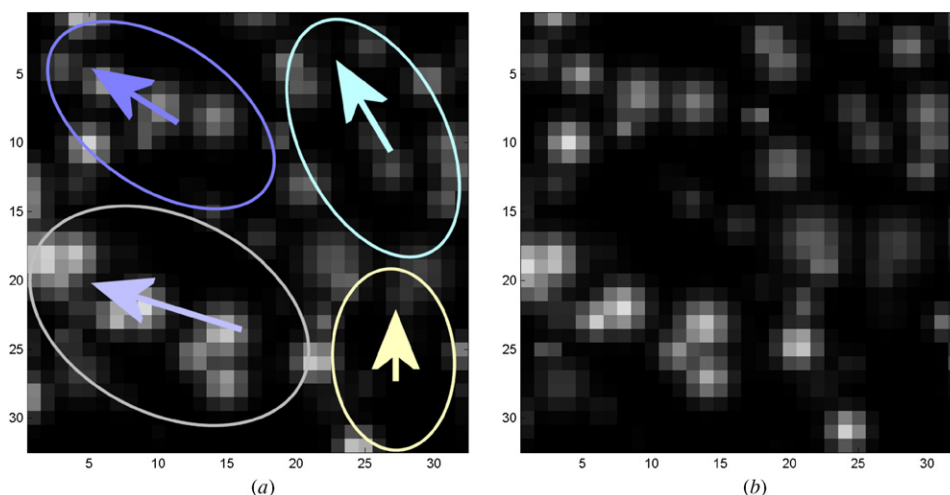


Figure 4. Image blocks undergoing nonlinear motion. (a) Block from image 1. (b) Block from image 2.

The local motion field is obtained in a similar manner as the global motion estimation in that phase correlation is performed on a tessellation of blocks over the entire image. To improve the accuracy of the estimate, the position of the peaks obtained by phase correlation is verified by comparing the position of the peak from the cross correlation surface, $\Psi(\mathbf{d}) = [E(\mathbf{x}, t) - \overline{E(\mathbf{x}, t)}][E(\mathbf{x}', t + \Delta t) - \overline{E(\mathbf{x}', t + \Delta t)}]$.

Both Ψ and \wp can be computed from the Fourier transform of the image block and each is used to cross verify the accuracy of the other. If the positions of the two peaks are unchanged, the estimate can be considered a very reliable estimate within the region of comparison as shown in figure 3. Thus, it provides a strong verification metric on the reliability of the estimate.

The presence of a mismatch between the peaks indicates the possibility that the region under consideration has significant nonlinear motion. This is evident from the affine Fourier theorem (6), where the affine parameters affect the phase term to a greater extent. This can be seen in figure 4, where two interrogation blocks from a region undergoing

motion are shown. Regions shown in the ellipses have been picked manually to give an indication of the nonlinear motion taking place within the region.

Given the two image blocks (figure 4), the peaks of the cross correlation and phase correlation have a positional mismatch and as can be seen in figure 5, the maximum of the phase correlation has another strong component in the vicinity. This positional mismatch indicates the possibility of multiple motions being present in the interrogation blocks. Any linear region-based scheme would provide an average estimate of the motion within the window which would be inaccurate.

To rectify this, we compute a set of potential candidates from the phase correlation and cross correlation surfaces if there is a mismatch between the peaks

$$C = \{\text{phase}_i\} \cup \{\max(\Psi(\mathbf{d}))\} \quad (7)$$

where $\text{phase}_i = \kappa \max(\wp(\mathbf{d}))$ are the positional candidates from the phase correlation surface (From experimentation we found that $\kappa = 0.75$ provides reasonable candidates) and

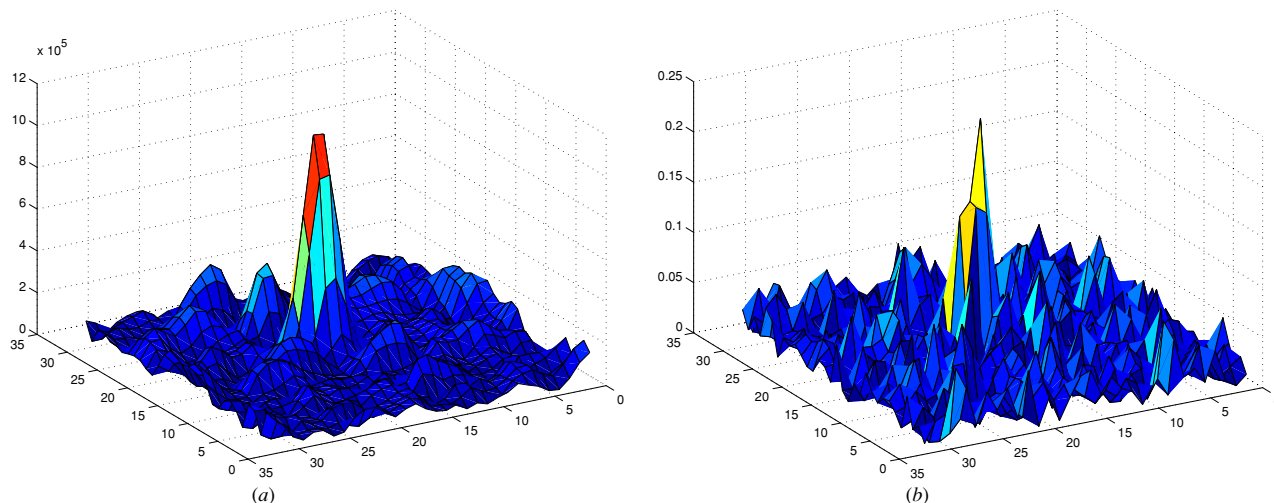


Figure 5. Peak mismatch indicating strong nonlinear motion using (a) cross correlation (b) phase correlation.

$\max(\Psi(\mathbf{d}))$ is the position of the maximum from the cross correlation surface³.

The best candidate is then obtained by computing ‘normalized cross correlation’ (ρ) at these candidate estimates (C) and selecting the candidate having the highest value of ρ . This technique does not provide the parametrization of the higher order motion model but nevertheless, within the constraint of a piecewise linear motion model, the method provides the most robust solution possible. Thus, instead of computing ρ at every pixel within the interrogation blocks, the algorithm selects a set of candidates to determine the best among them.

The flow chart for the local piecewise linear motion estimation is provided in figure 6. As explained before, computational complexity in computing the two metrics (Ψ and ρ) does not increase significantly since this could be accomplished by performing the Fourier transform only once over the regions under consideration.

Having obtained the integer resolution motion field, sub-pixel level motion interpolation is done by fitting a 3-point Gaussian fit [43] over the normalized cross correlation (ρ) values in the neighbourhood of the best estimate, where the sub-pixel estimate (δ) is estimated by

$$\delta = \frac{\ln \rho_{-1} - \ln \rho_{+1}}{2(\ln \rho_{-1} + \ln \rho_{+1} - 2 \ln \rho_0)} \quad (8)$$

where ρ_{-1} , ρ_0 and ρ_{+1} are the estimates of the normalized cross correlation in the neighbourhood under consideration. As suggested by Marxen *et al* [25], a 3-point Gaussian fit was used in the sub-pixel estimation scheme due to the Gaussian profile of the particles in the images.

The main advantage of this scheme is the cross verification of the motion estimates using the results obtained from the phase correlation and cross correlation. This voting scheme improves the reliability of the estimated vectors over any one method applied alone.

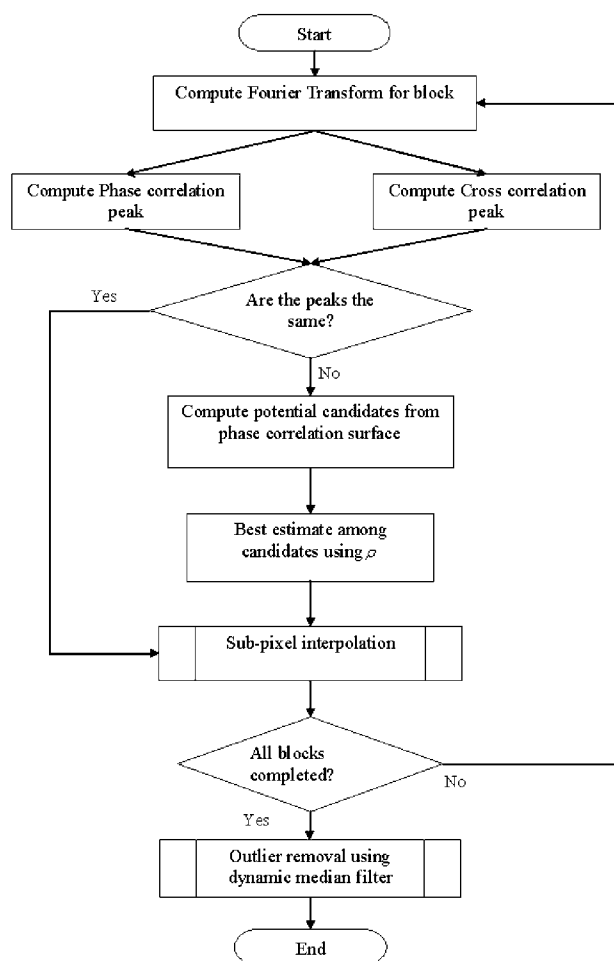


Figure 6. Flow chart for the estimation of the local motion field.

3.3. Outlier removal and de-noising

Though the voting scheme reduces the possibility of incorrect estimates, image regions containing low gradient information due to insufficient seeding could still provide incorrect estimates. Removal of these spurious vectors is done by using

³ The reason that the candidates are selected from the phase correlation surface as against the cross correlation is because of the reduced surface spread around each peak in the phase correlation surface.

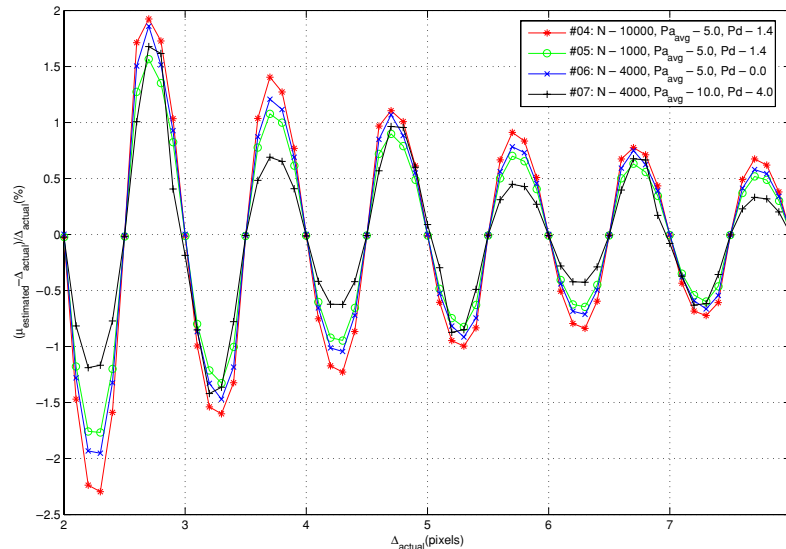


Figure 7. Variation of error under synthetic translation.

a modified median filter as proposed by Westerweel [41] where the velocity vector $U_{2D}(i, j)$ is considered valid if

$$|U_{2D}(\text{median}) - U_{2D}(i, j)| < \epsilon_{\text{threshold}} \quad (9)$$

where $U_{2D}(\text{median})$ is the median of the vectors in the neighbourhood of $U_{2D}(i, j)$ and $\epsilon_{\text{threshold}}$ determines the reliability of $U_{2D}(i, j)$. ($\epsilon_{\text{threshold}}$) was determined in a manner similar to the ‘dynamic mean value filter’ [32]. The standard deviation of the vectors in the neighbourhood, $\sigma_U(i, j)$, was used to weight two constants C_1 and C_2 as $C_1 + C_2\sigma_U(i, j)$ (for the dynamic median filter in the local motion estimation, the constants $C_1 = 0.6$ and $C_2 = 0.6$ were found sufficient for performing the outlier detection). From computations done with the standardized images, the ‘dynamic median value filter’ provided a better local neighbourhood filtering than the ‘dynamic mean value filter’.

4. Results and analysis

The algorithm has been implemented using a prototype written in Matlab 6.5 R13. For the global motion estimation, interrogation block sizes were maintained at a constant 32×32 pixels throughout the image hierarchy so as to obtain an amplified and accurate translation at the finer scales. For the local estimation, the interrogation block size was 16×16 pixels. Both global and local estimations were performed with a 50% overlap between adjacent blocks.

At each level of the image pyramid, the global motion field was median filtered using a 3×3 motion field neighbourhood. Thus, the motion field was smoothed over larger motion estimates at coarser levels of the pyramid when compared to the finer resolutions. This over-smoothing of the global motion field provided for the smoothness regularization in the estimation of the motion.

4.1. Standard images—JPIV (PIV-STD project)

The images used for the validation of the algorithm were obtained from the JPIV (PIV-STD project) [27]. In applying

the algorithm for standard images from JPIV, both the non-transient and transient cases have been evaluated to determine the utility of this method.

As described by Prasad [29], bias errors in the estimation process degrade the accuracy of the estimated flow field. An important part of a PIV algorithm is its ability to minimize the bias errors, specifically peak locking, robustly [16]. In investigating the robustness of the method described in handling the bias errors, the standard images were warped using known translations and the motion was estimated.

4.1.1. Synthetic translation. In quantifying the errors that arise either due to the estimation process or the sub-pixel estimation technique, the first step would be to estimate known sub-pixel motion using the proposed method. To this end, four specific JPIV test cases (#004, #005, #006, #007) were warped, using bilinear interpolations, with translations from the range [2.0, 2.1, . . . , 8.0]. The four test cases account for a typical displacement/seeding density scenario in a standard PIV experiment and thus have been used to verify the processing method.

- JPIV transient test #004: high particle seeding density ($N = 10000$)
- JPIV transient test #005: low particle seeding density ($N = 1000$)
- JPIV transient test #006: constant particle size ($Pa_{\text{avg}} = 5.0, Pd = 0.0$)
- JPIV transient test #007: large particle size ($Pa_{\text{avg}} = 10.0, Pd = 4.0$)

Histogram plots for a few of the translations are shown in figure 8 and as can be seen from the plots, the sub-pixel estimator is considerably robust. Though the existence of peak locking cannot be ruled out completely when using the standard Gaussian interpolation function [34], the most important point to be considered in analysing sub-pixel estimators is the error significance which can be obtained as the ratio between the deviation and the actual translation. This is evident in figure 7 where the percentage deviation has been

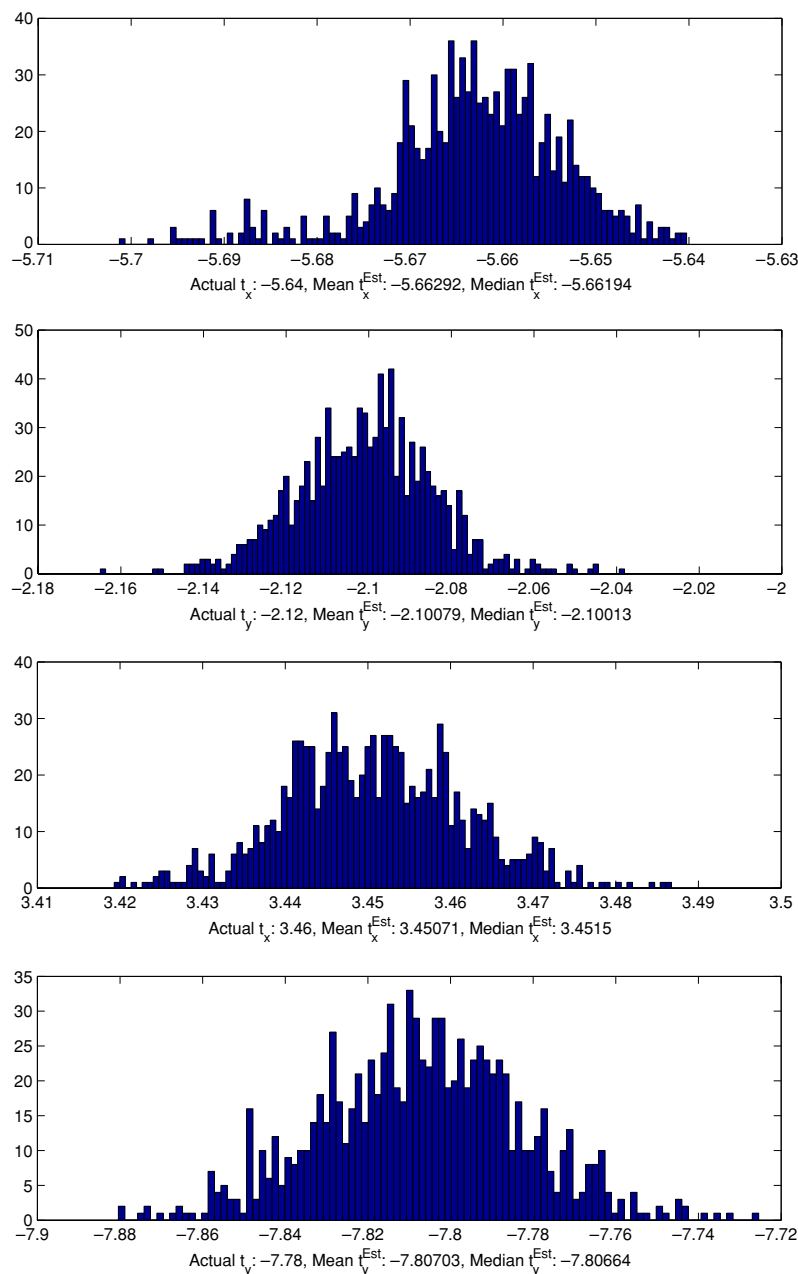


Figure 8. Histogram plots of the estimated displacements.

plotted for the four test cases. The presence of the signal oscillations indicates the presence of peak locking but as can be seen, the amplitude of the oscillations is within 2% of the actual displacement range.

The bias error variations, with increasing/decreasing seeding density and/or the pixel diameter, agree with trends observed by Collicott [10] and Prasad *et al* [29]. With an increased seeding density (SD), the error seems larger than with lower SD. With increasing particle size, the bias error deviations decrease, with bias error being zero at full pixel and half pixel resolutions. The above results were obtained by running the simulations using an interrogations window size of 16×16 pixels with 50% overlap.

Shown in figure 8 are the histogram plots for a few selected displacements in the X and Y directions. The histograms have

been computed from the JPIV test case #07 by warping the two images by the displacement indicated by ‘Actual t_x/t_y ’ and the velocity estimates have been computed using a 16×16 pixel interrogation window with 50% overlap.

4.1.2. Non-transient case. Figure 9 is a sample scatter plot obtained from the magnitude and phase variation between the estimated and the ground truth displacement vectors for spatially collocated positions.

The green markers in the scatter plots are the vectors whose magnitude is within 1 pixel difference from the standardized vectors while the red markers indicate those estimates that deviate from the standardized vector by more than 1 pixel in magnitude. In tables 1 and 2, $n_{complete}$ are the total number of estimates which have been compared with the

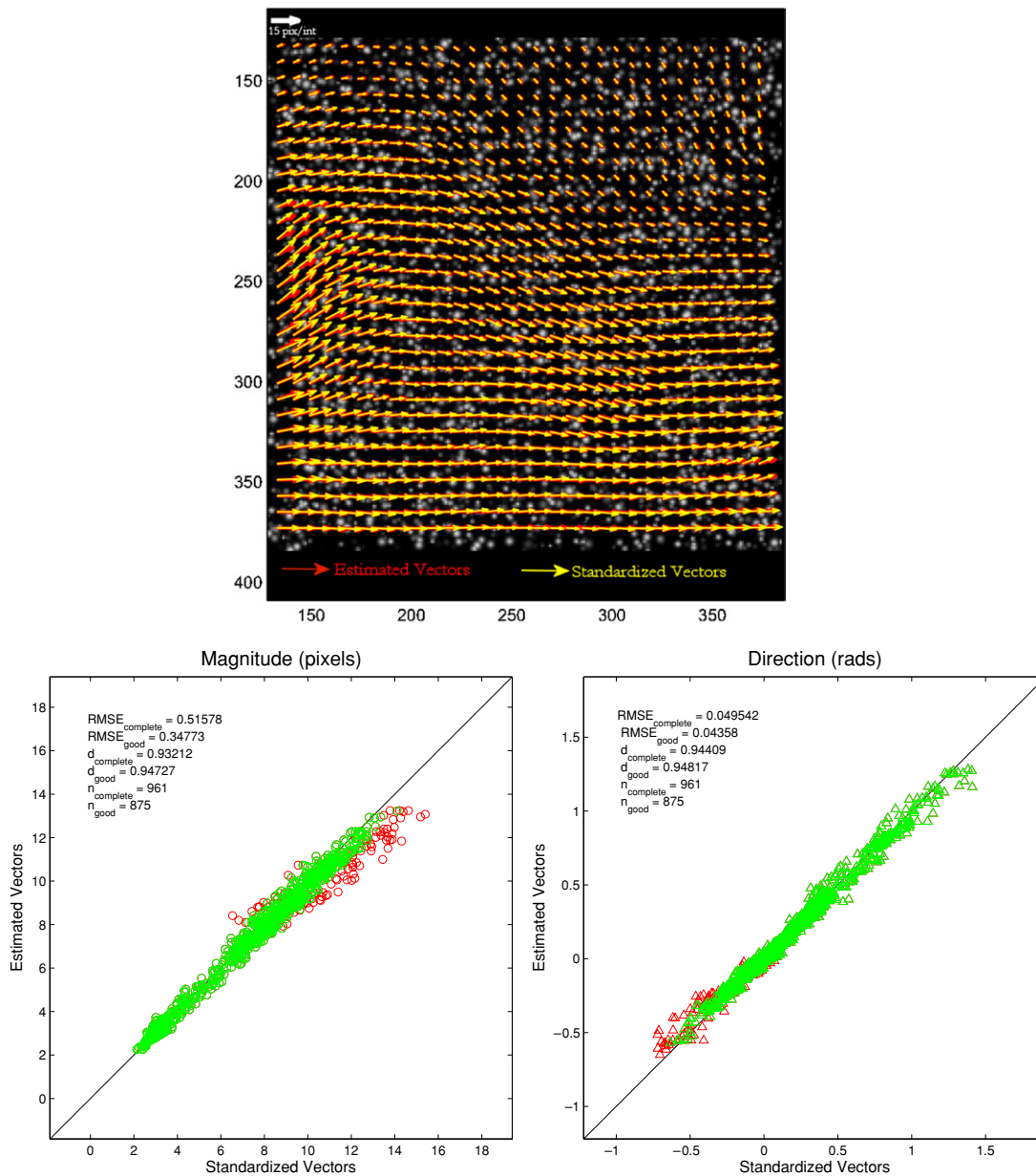


Figure 9. Estimated vectors versus standardized vectors for JPIV test case #001.

Table 1. Comparison of magnitude (in pixels) between the standardized vectors and estimated vectors.

Test no	n_{complete}	n_{good}	$RMSE_{\text{complete}}$	$RMSE_{\text{good}}$	d_{complete}	d_{good}
1	961.0000	875.0000	0.5158	0.3477	0.9321	0.9473
2	961.0000	179.0000	11.8954	0.3596	0.5834	0.9541
3	961.0000	960.0000	0.2517	0.2503	0.8745	0.8749
4	961.0000	909.0000	0.4425	0.3261	0.9436	0.9530
5	961.0000	838.0000	0.5560	0.3661	0.9274	0.9478
6	961.0000	893.0000	0.5160	0.3261	0.9369	0.9516
7	961.0000	906.0000	0.4399	0.3255	0.9421	0.9515
8	961.0000	856.0000	0.5376	0.3431	0.9305	0.9491

ground truth vectors and n_{good} constitute the estimated vectors that are within 1 pixel difference from the ground truth. (n_{complete} and n_{good}).

Two statistical measures of the similarity, the root mean square error and the index of agreement [44], have been computed for the magnitude and the phase variation (for both

$$RMSE = \sqrt{\frac{1}{K} \sum_{k=1}^K (p_k - o_k)^2} \quad (10)$$

Table 2. Comparison of direction (in rads) between the standardized vectors and estimated vectors.

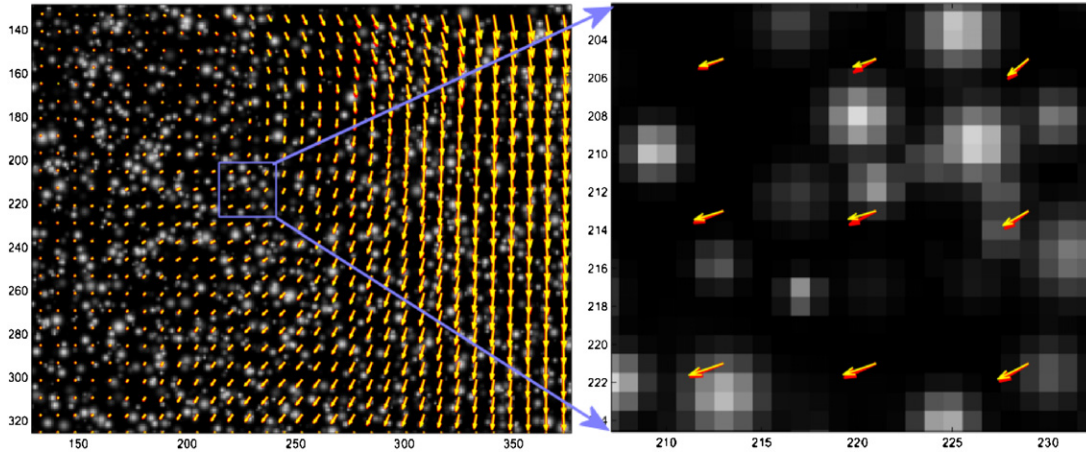
Test no	n_{complete}	n_{good}	$RMSE_{\text{complete}}$	$RMSE_{\text{good}}$	d_{complete}	d_{good}
1	961.0000	875.0000	0.0495	0.0436	0.9441	0.9482
2	961.0000	179.0000	1.5934	0.0414	0.3317	0.9363
3	961.0000	960.0000	0.0456	0.0453	0.9477	0.9479
4	961.0000	909.0000	0.0424	0.0393	0.9520	0.9543
5	961.0000	838.0000	0.0593	0.0522	0.9331	0.9403
6	961.0000	893.0000	0.0427	0.0394	0.9504	0.9528
7	961.0000	906.0000	0.0451	0.0436	0.9489	0.9502
8	961.0000	856.0000	0.0538	0.0464	0.9382	0.9441

Table 3. Comparison of magnitude (in pixels) between the standardized vectors and estimated vectors of #301.

Test no	n_{complete}	n_{good}	$RMSE_{\text{complete}}$	$RMSE_{\text{good}}$	d_{complete}	d_{good}
11	961.0000	942.0000	0.1419	0.1220	0.9758	0.9772
12	961.0000	933.0000	0.1591	0.1302	0.9738	0.9759
57	961.0000	889.0000	0.2472	0.1511	0.9686	0.9766
86	961.0000	935.0000	0.1690	0.1133	0.9731	0.9767

Table 4. Comparison of direction (in rads) between the standardized vectors and estimated vectors of #301.

Test no	n_{complete}	n_{good}	$RMSE_{\text{complete}}$	$RMSE_{\text{good}}$	d_{complete}	d_{good}
11	961.0000	942.0000	0.0661	0.0657	0.9489	0.9504
12	961.0000	933.0000	0.0726	0.0721	0.9464	0.9484
57	961.0000	889.0000	0.0896	0.0847	0.9308	0.9335
86	961.0000	935.0000	0.0694	0.0680	0.9292	0.9307

**Figure 10.** Estimated vectors versus standardized vectors for the transient case.

$$d_\gamma = 1 - \left[\sum_{k=1}^K \omega_k (p_k - o_k)^\gamma \right] \times \left[\sum_{k=1}^K \omega_k (|p_k - \bar{o}| + |o_k - \bar{o}|)^\gamma \right]^{-1} \quad (11)$$

p_k are the predicted vectors, o_k are the observed ground truth vectors, w_k are the weight functions which are assumed uniform for this study, \bar{o} is the mean of the ground truth data and K are the total number of vectors being compared. γ is the order of index and according to Willmott [44], $\gamma = 1$ is most robust for comparing results because of its linear approach to a perfect match.

As can be observed, the algorithm provides accurate estimates when compared to the ground truth vectors for all image pairs, except image no 2. The main reason for this was due to the large non-rigid motion present in the image

pair. Most region-based techniques fail for this pair of images because of the extreme changes in the position of the particles and the gradient of the velocity vectors.

4.1.3. Transient case. The test cases for the transient flow were obtained from image test no 301 (transient 3D flow field with slit light sheet) with 4000 particles. As in the previous section, the comparative results of the transient case have been provided in tables 3 and 4. The ‘good’ estimates in the transient cases are the estimated vectors having a magnitude difference of less than 0.5 pixels with the ground truth vectors. As can be seen from results, the algorithm provides accurate estimates.

A common trend among the transient test cases is the increased $RMSE$ in the directional components with the magnitude differences remaining small. This is due to the sub-pixel level vector differences and is shown in figure 10. As can

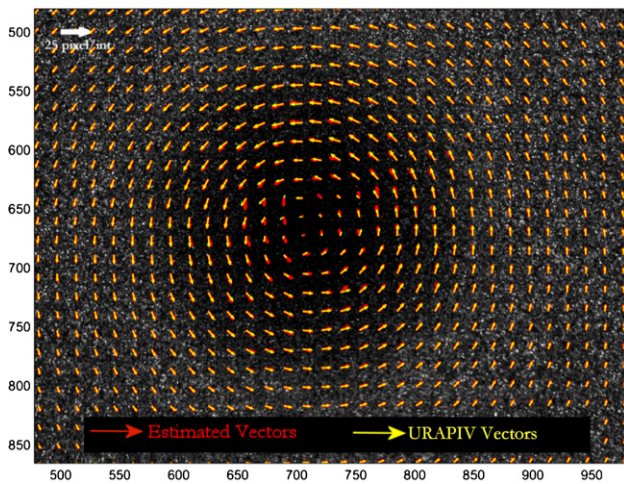


Figure 11. Estimated vectors for the PIV Challenge test case A: estimated vectors along with the URAPIV vectors using an interrogation window of 32×32 pixels with 50% overlap.

be observed, though the magnitude of the estimated vectors is less than 0.5 pixels from the ground truth vectors, due to sub-pixel differences the *RMSE* for the directional differences is large.

4.2. Standard images—PIV Challenge 2001

The algorithm has also been tested for the data from the PIV Challenge 2001 [37]. The two data sets available for download are the test cases A and B. In testing the validity of the technique for the images from the PIV Challenge, the results obtained have been compared with URAPIV routine [21] due to unavailability of ground truth motion vectors.

4.2.1. Case A. This test case (provided by Christian Kaehler) was obtained from the recording of a wake vortex formation behind a transport aircraft (DLR ALVAST half model) in landing configuration (<http://www.pivchallenge.org/pub/readmeA.txt>). The estimated vectors have been compared with the vectors obtained from the URAPIV routine using an interrogation window of 32×32 pixels with 50% overlap. The output shown in figure 11 shows the motion field as estimated from the image pair.

4.2.2. Case B. The synthesized test case (provided by Okamoto) shows a strong vortex obtained with different seeding densities and different particle image sizes (<http://www.pivchallenge.org/pub/readmeB.txt>). Shown in figure 12 is the estimated motion field under the constraint of small particle size (particle image diameter—1.8 pixels) and low seeding density. Also shown are the vectors estimated using the URAPIV routine using 32×32 pixel interrogation window with 50% overlap. In spite of the low seeding density, the estimated vectors correspond very well with the URAPIV vectors.

5. Discussions

A significant component of the present algorithm is the voting scheme, which is used to improve the reliability of the

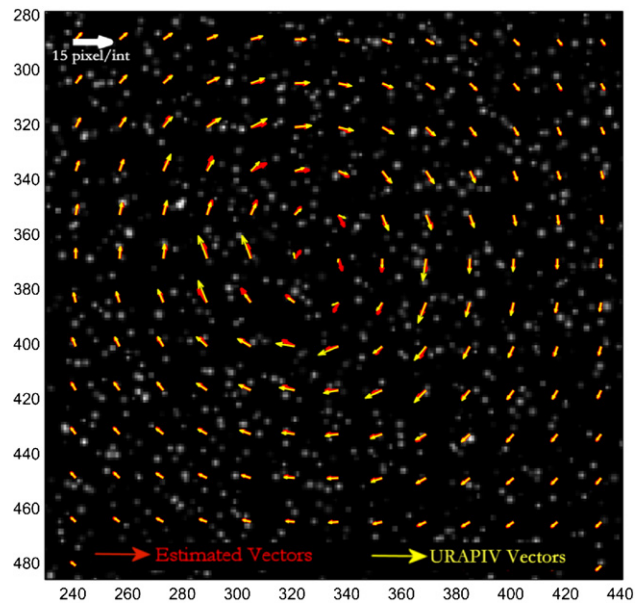


Figure 12. Estimated vectors from the PIV Challenge test case B: small particle size and low seeding density.

estimated vectors. Cross correlation in itself is not illumination invariant, but in combination with an illumination invariant metric such as phase correlation, it provides a more accurate estimation of the observed flow. The method belongs to a class of region-based motion estimation methods [5] and the optimal solution is defined under the constraint of a region-based metric. The solution obtained by the algorithm can thus be considered the best possible under the constraints of a region-based correlation assumption.

One of the advantages of using the hierarchical two-stage estimation technique is the possibility of obtaining a smooth and accurate motion field at high resolution. This is shown in figure 13, where motion has been estimated accurately using an interrogation window up to 8×8 pixels with a 50% overlap. Under similar constraint of 50% overlap, the vectors estimated using the URAPIV routine are also shown. This accurate motion estimation is due to the initialization of the local motion field estimation using the global motion. Thus, the coarse global motion guides the high resolution local motion accurately.

The URAPIV routine provides accurate estimates at 32×32 pixel blocks but at higher resolution the estimates obtained cannot be considered accurate as shown in figure 13. The technique described in this paper provides accurate estimates at a pixel resolution of 8×8 pixel blocks using a 50% overlap as shown in figure 14.

In terms of the computational efficiency, the current implementation of the algorithm requires ~ 12.5 s to process 4096 vectors using an interrogation window size of 8×8 pixel with 50% overlap. The simulation was performed on a P4, 2.4 GHz PC with the code implemented in Matlab 6.5 R13. This could obviously be greatly improved by using an optimized ‘C’ implementation of the same.

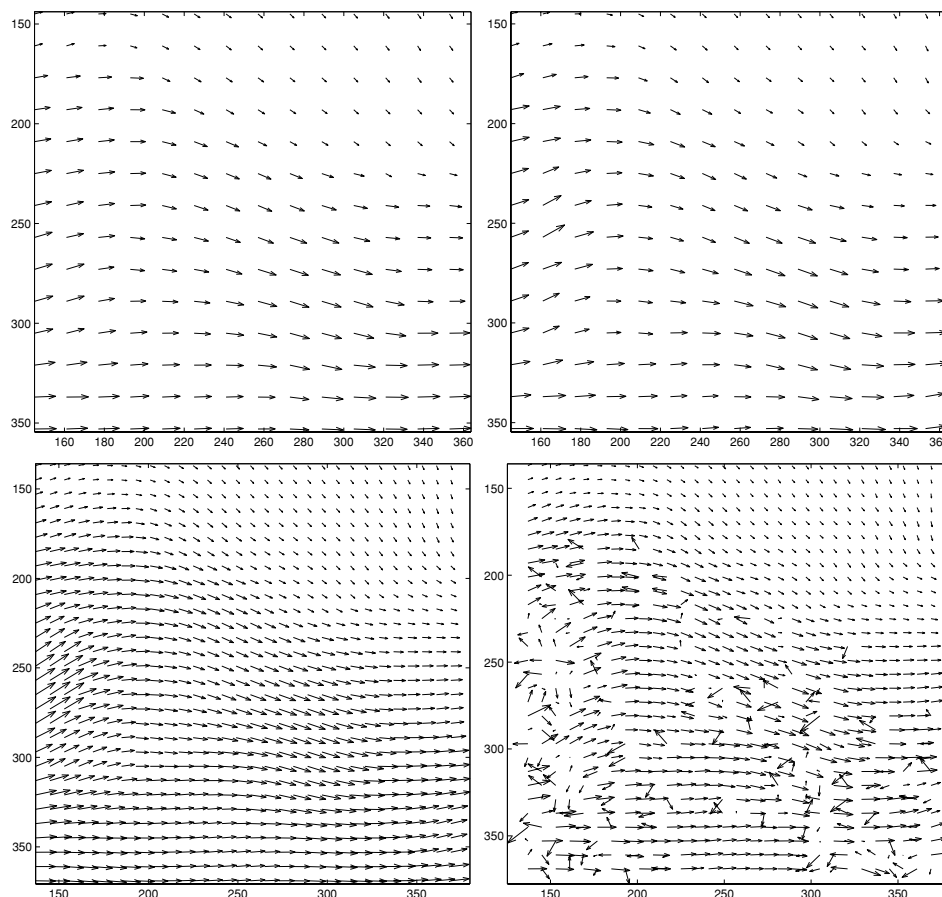


Figure 13. Estimated output for standardized images, test no 1. Row 1: interrogation window of 32×32 pixels. Row 2: interrogation window of 16×16 pixels. Column 1: estimated vectors. Column 2: URAPIV vectors.

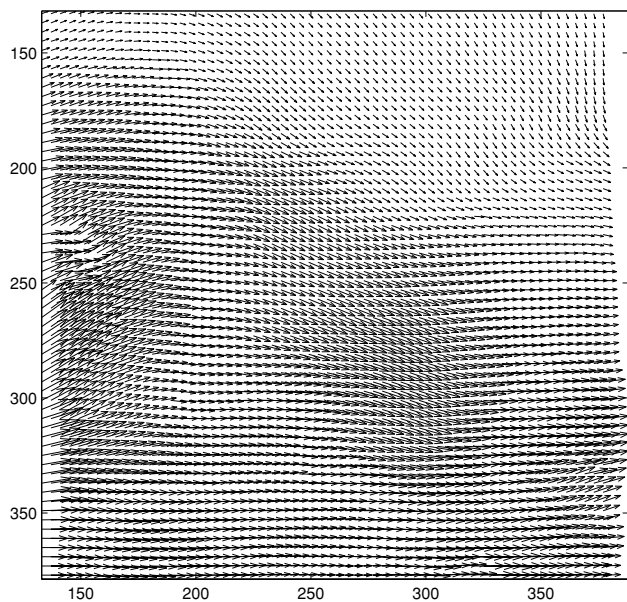


Figure 14. Estimated output for standardized images, test no 1 for 8×8 pixels resolution.

6. Conclusions

We have implemented an algorithm by which the motion estimation on PIV data sets can be performed reliably and

robustly. This algorithm is composed of a two-stage technique, the global motion field estimation followed by local differential motion estimation, to provide the best possible estimate that can be obtained using region-based schemes.

The comparative results between the estimated vectors and the ground truth vectors indicate that the hierarchical phase correlation is quite accurate for the estimation of the motion. This is mainly due to the inherent robustness of phase correlation to illumination variation. Additionally, the usage of the fast Fourier transform in the calculation of the phase correlation term makes the computation significantly faster than most differential techniques.

The reliability metric developed for this algorithm, based on voting using phase correlation and cross correlation metrics, provides reliable and accurate information in determining positions of a significant number of outliers. This prevents over-smoothing of the motion field, which would be the case otherwise if smoothing filters are used.

Results from the JPIV standardized images appear promising in the utilization of this technique in estimating motion in PIV imagery. This is also evident in the dispersion of the estimated vectors with respect to the ground truth vectors in the magnitude and phase scatter plots.

As a subsequent stage to the current research, the estimate of the local deformation could be improved using an explicit regularization parameter. Another possible track for future research would be to estimate higher order motion, such as quadratic, in the regions where the linear motion model

collapses followed by a quad-tree based decomposition to estimate the best possible motion field.

Acknowledgments

Research funding was provided by the National Ocean Partnership Programme (NOPP) N00014-99-1-1051 and National Science Foundation grant CAREER IRI-9984842.

References

- [1] Adrian R J 1984 Scattering particle characteristics and their effect on pulsed laser measurements of fluid flow: speckle velocimetry vs. particle image velocimetry *Appl. Opt.* **23** 1690–1
- [2] Adrian R J 1991 Particle-imaging technique for experimental fluid mechanics *Annu. Rev. Fluid Mech.* **23** 261–304
- [3] Anandan P 1989 A computational framework and an algorithm for the measurement of visual motion *Int. J. Comput. Vis.* **2** 283–310
- [4] Anandan P *et al* 1992 Hierarchical model-based motion estimation *Proc. European Conf. on Computer Vision* p 237–52
- [5] Barron J L *et al* 1994 Performance of optical flow techniques *Int. J. Comput. Vis.* **12** 43–77
- [6] Black M J 1992 Robust incremental optic flow *PhD Thesis* Yale University
- [7] Burt P J and Adelson E H 1983 The Laplacian Pyramid as a compact image code *IEEE Trans Commun.* **31** 532–40
- [8] Bracewell R N 1993 Affine theorem for two-dimensional Fourier transform *Electron. Lett.* **29** 304
- [9] Christensen K T 2004 The influence of peak-locking errors on turbulence statistics computed from PIV ensembles *Exp. Fluids* **36** 484–97
- [10] Collicott S H 1993 Transition from particle image velocimetry to laser speckle velocimetry with increasing seeding density *Applications of Laser Techniques to Fluid Mechanics* (Berlin: Springer) pp 181–94
- [11] Cooley J W and Tukey J W 1965 An algorithm for the machine calculation of complex Fourier series *Math. Comput.* **19** 297–301
- [12] Corpetti T *et al* 2002 Dense estimation of fluid flows *IEEE Trans. Pattern Anal. Mach. Intell.* **24** 365–80
- [13] Forrosh H *et al* 2002 Extension of phase correlation to subpixel registration *IEEE Trans. Image Process.* **11** 188–200
- [14] Green R B *et al* 2000 Measurements of the orthogonal blade-vortex interaction using a particle image velocimetry technique *Exp. Fluids* **29** 369–79
- [15] Gui L and Wereley S T 2002 A correlation-based continuous window-shift technique to reduce the peak-locking effect in digital PIV image evaluation *Exp. Fluids* **32** 506–17
- [16] Huang H *et al* 1997 On errors of digital particle image velocimetry *Meas. Sci. Technol.* **8** 1427–40
- [17] Horn B K P and Schunck B G 1981 Determining optical flow *Artif. Intell.* **17** 185–203
- [18] Bolinder J 1999 On the accuracy of a digital particle image velocimetry system *Technical Report* Lund Institute of Technology, Sweden ISSN 0282-1990
- [19] Keane R D and Adrian R J 1992 Theory of cross-correlation analysis of PIV images *Appl. Sci. Res.* **49** 191–215
- [20] Kruger S A and Calway A D 1996 A multiresolution frequency domain method for estimating affine motion parameters *Int. Conf. on Image Processing* pp 113–6
- [21] Liberzon A *et al* 2001 Vorticity characterization in a turbulent boundary layer using PIV and POD analysis *4th Int. Symp. on Particle Image Velocimetry*
- [22] Lourenco L and Krothapalli A 1995 On the accuracy of velocity and vorticity measurements with PIV *Exp. Fluids* **13** 421–8
- [23] Lucchese L 2001 A frequency domain technique based on energy radial projections for robust estimation of global 2D affine transformations *Comput. Vis. Image Underst.* **81** 72–116
- [24] Manduchi R and Mian G A 1993 Accuracy analysis for correlation-based image registration algorithms *Proc. ISCAS* pp 834–7
- [25] Marxen M *et al* 2000 Comparison of Gaussian particle centre estimators and the achievable measurement density for particle tracking velocimetry *Exp. Fluids* **29** 145–53
- [26] Nogueira J *et al* 1997 Data validation, false vectors correction and derived magnitudes calculation on PIV *Meas. Sci. Technol.* **8** 1493–501
- [27] Okamoto K *et al* 2000 Standard images for particle-image velocimetry (www.vsj.or.jp/piv/) *Meas. Sci. Technol.* **11** 685–91
- [28] Prasad A K 2000 Particle image velocimetry (invited review paper) *Curr. Sci.* **79** 101–10
- [29] Prasad A K *et al* 1992 Effect of resolution on the speed and accuracy of particle image velocimetry interrogations *Exp. Fluids* **13** 105–16
- [30] Proakis J G and Manolakis D G 1995 *Digital Signal Processing: Principles, Algorithms and Applications* (Englewood Cliffs, NJ: Prentice Hall)
- [31] Quenot G M *et al* 1998 Particle image velocimetry with optical flow *Exp. Fluids* **25** 177–89
- [32] Raffel M *et al* 1998 *Particle Image Velocimetry—A Practical Guide* (Berlin: Springer)
- [33] Reddy B and Chatterji B 1996 An FFT-based technique for translation, rotation, and scale-invariant image registration *IEEE Trans. Image Process.* **5** 1266–71
- [34] Roesgen T 2003 Optimal subpixel interpolation in particle image velocimetry *Exp. Fluids* **35** 252–6
- [35] Scarano F and Riethmuller M L 1999 Iterative multigrid approach in PIV image processing with discrete window offset *Exp. Fluids* **26** 513–23
- [36] Scarano F 2002 Iterative image deformation methods in PIV *Meas. Sci. Technol.* **13** R1–19
- [37] Stanislas M *et al* 2003 Main results of the first international PIV challenge (www.pivchallenge.org/) *Meas. Sci. Technol.* **14** R63–89
- [38] Thomas G A 1987 Television motion measurement for DATV and other applications, BBC Research Department
- [39] Truco E and Verri A 1998 *Introductory Techniques for 3-D Computer Vision* (Englewood Cliffs, NJ: Prentice Hall)
- [40] Vernon D 2001 *Fourier Vision—Segmentation and Velocity Measurement using Fourier Transform* (Dordrecht: Kluwer)
- [41] Westerweel J 1994 Efficient detection of spurious vectors in particle image velocimetry data *Exp. Fluids* **16** 236–47
- [42] Westerweel J 1997 Fundamentals of digital particle image velocimetry *Meas. Sci. Technol.* **8** 1379–92
- [43] Willert C E and Gharib M 1991 Digital particle image velocimetry *Exp. Fluids* **10** 181–93
- [44] Willmot C J *et al* 1985 Statistics for the evaluation and comparison of models *J. Geophys. Res.* **90** 8995–9005